^{18}F-ICMT-11, a Caspase-3–Specific PET Tracer for Apoptosis: Biodistribution and Radiation Dosimetry

Amarnath Challapalli[1], Laura M. Kenny[1], William A. Hallett[2], Kasia Kozlowski[1], Giampaolo Tomasi[1], Mihir Gudi[1], Adil Al-Nahhas[3], R. Charles Coombes[1], and Eric O. Aboagye[1]

[1]Department of Surgery and Cancer, Imperial College London, London, United Kingdom; [2]Imanova Centre for Imaging Studies, London, United Kingdom; and [3]Department of Radiology/Nuclear Medicine, Imperial College Healthcare NHS Trust, London, United Kingdom

Effective anticancer therapy induces tumor cell death through apoptosis. Noninvasive monitoring of apoptosis during therapy may provide predictive outcome information and help tailor treatment. A caspase-3–specific imaging radiotracer, ^{18}F-(*S*)-1-((1-(2-fluoroethyl)-1H-[1,2,3]-triazol-4-yl)methyl)-5-(2(2,4-difluorophenoxymethyl)-pyrrolidine-1-sulfonyl)isatin (^{18}F-ICMT-11), has been developed for use in PET studies. We report the safety, biodistribution, and internal radiation dosimetry profiles of ^{18}F-ICMT-11 in 8 healthy human volunteers. **Methods:** ^{18}F-ICMT-11 was intravenously administered as a bolus injection (mean ± SD, 159 ± 2.75 MBq; range, 154–161 MBq) to 8 healthy volunteers (4 men, 4 women). Whole-body (vertex to mid thigh) PET/CT scans were acquired at 6 time points, up to 4 h after tracer injection. Serial whole blood, plasma, and urine samples were collected for radioactivity measurement and radiotracer stability. In vivo ^{18}F activities were determined from quantitative analysis of the images, and time–activity curves were generated. The total numbers of disintegrations in each organ normalized to injected activity (residence times) were calculated as the area under the curve of the time–activity curve, normalized to injected activities and standard values of organ volumes. Dosimetry calculations were then performed using OLINDA/EXM 1.1. **Results:** Injection of ^{18}F-ICMT-11 was well tolerated in all subjects, with no serious tracer-related adverse events reported. The mean effective dose averaged over both men and women was estimated to be 0.025 ± 0.004 mSv/MBq (men, 0.022 ± 0.004 mSv/MBq; women, 0.027 ± 0.004 mSv/MBq). The 5 organs receiving the highest absorbed dose (mGy/MBq), averaged over both men and women, were the gallbladder wall (0.59 ± 0.44), small intestine (0.12 ± 0.05), upper large intestinal wall (0.08 ± 0.07), urinary bladder wall (0.08 ± 0.02), and liver (0.07 ± 0.01). Elimination was both renal and via the hepatobiliary system. **Conclusion:** ^{18}F-ICMT-11 is a safe PET tracer with a dosimetry profile comparable to other common ^{18}F PET tracers. These data support the further development of ^{18}F-ICMT-11 for clinical imaging of apoptosis.

Key Words: ^{18}F-ICMT-11; caspase-3; apoptosis; biodistribution; dosimetry

J Nucl Med 2013; 54:1551–1556
DOI: 10.2967/jnumed.112.118760

Apoptosis is an essential process for eliminating unwanted cells during embryonic development, growth, differentiation, and maintenance of tissue homeostasis. Apoptosis is regulated by both intrinsic (via mitochondria) and extrinsic (activation of death receptors) signaling networks that control a family of enzymes known as caspases (cysteine aspartate specific proteases) (*1,2*). The pathways activate initiator caspases 8 (extrinsic) or 9 (intrinsic), which in turn cleave the inactive procaspases 3, 6, and 7 into the active executioner caspases-3, -6, and -7 (*3*). Deregulation of apoptosis signaling pathways is therefore associated with various pathologies—including autoimmunity, neurodegeneration, cardiac ischemia, and transplant rejection (*4*)—and the capacity to evade apoptosis has been defined as one of the hallmarks of cancer (*5*).

In cancer, apoptosis is induced by a large variety of stimuli including cytotoxic and mechanism-based therapeutics and radiotherapy. Although those stimuli trigger different apoptotic signaling pathways, the molecular events in the execution phase of apoptosis are largely shared and involve caspases. Within the caspase family, the effector caspases (caspases-3, -6, and -7) orchestrate the demolition phase of apoptosis that results in the controlled dismantling of a range of key structures within the cell and its subsequent disposal (*6*). Moreover, one of the most noticeable and specific features of apoptosis is the degradation of the DNA into numerous fragments, often down to multiples of 200 base pairs, driven by the activation of caspase-3 (*7*), the central effector caspase, which makes it an attractive biomarker of apoptosis.

Effective anticancer therapy often requires induction of tumor cell death through apoptosis. Monitoring of this process could provide important predictive outcome information in the context of routine patient management and early clinical trials (*8,9*). The apoptotic index has been shown to correlate with chemotherapy efficacy and to be of prognostic significance (*10,11*). A noninvasive apoptosis imaging technology such as PET could permit the detection of biologic changes in the tumor that evolve over hours of initiating treatment. This shorter time frame is in contrast to changes in tumor size that evolve over months, which forms the basis for Response Evaluation Criteria in Solid Tumors guidelines (*12*).

On the basis of various biochemical events that characterize apoptosis, several positron-emitting radiotracers have been developed to noninvasively detect this process, both in preclinical studies and in humans (*13*). ^{18}F-(*S*)-1-((1-(2-fluoroethyl)-1H-[1,2,3]-triazol-4-yl) methyl)-5-(2(2,4-difluorophenoxymethyl)-pyrrolidine-1-sulfonyl) isatin (^{18}F-ICMT-11) was designed as a small-molecule radiotracer with potential advantages such as facile radiolabeling and improved

Received Dec. 19, 2012; revision accepted Apr. 12, 2013.
For correspondence or reprints contact: Eric Aboagye, Department of Surgery and Cancer, Imperial College London, Hammersmith Hospital, Du Cane Rd., London W12 0NN, U.K.
E-mail: eric.aboagye@imperial.ac.uk
Published online Aug. 15, 2013.

biodistribution and clearance profiles. It has been characterized as a novel reagent designed to noninvasively image caspase-3 activation and, hence, drug-induced apoptosis. We have validated ^{18}F-ICMT-11 as a caspase-3–specific PET imaging radiotracer for the assessment of tumor apoptosis preclinically in murine lymphoma xenografts treated with cyclophosphamide (*14*).

The promising mechanistic and biologic profile of ^{18}F-ICMT-11 supports its transition into clinical development (*13*). We present the first, to our knowledge, human study with ^{18}F-ICMT-11, performed with healthy volunteers, to evaluate the dosimetry, biodistribution, and safety of this tracer.

MATERIALS AND METHODS

Radiopharmaceutical Preparation

^{18}F-ICMT-11 was synthesized from the precursor as previously described (*15*). The radiochemical purity of ^{18}F-ICMT-11 was 100%, with a mean (±SD) specific activity of 1,951.5 ± 4,084 GBq/μmol (range, 110–12,032 GBq/μmol; the high specific activity in 1 subject was due to a lower cold concentration of ^{18}F-ICMT-11, below the limit of quantification) and a pH of 5.41 ± 0.16 (range, 5.16–5.71).

Subjects

Eight healthy volunteers (4 men, 4 women), with a mean age of 63.1 ± 2.58 y (range, 59–68 y) and an average weight of 74 ± 15.4 kg (range, 52.1–98.7 kg), were enrolled. Inclusion criteria included age above 50 y, the ability to provide informed written consent, and a normal medical history (including physical examination, electrocardiogram, hematology, and biochemistry). Exclusion criteria included pregnancy and lactation. No specific fasting or food protocol was implemented for subjects. Ethical approval for the study was granted by the West-London Research Ethics Committee. All volunteers gave written informed consent to participate in the study, according to the Declaration of Helsinki guidelines. The administration of radioactivity for the PET/CT scans was approved by the Administration of Radioactive Substances Advisory Committee, United Kingdom.

Safety

Safety data collected up to 72 h after injection included adverse events (AEs), graded according to common toxicity criteria (version 4.03; http://www.eortc.be/services/doc/ctc/CTCAE_4.03_2010-06 14_QuickReference_5x7.pdf); vital signs (blood pressure, respiratory rate, heart rate, and body temperature); physical examination; cardiovascular, lung, abdomen, and neurologic examinations; electrocardiogram; and laboratory parameters (serum biochemistry, hematology, coagulation, and urinalysis). Blood samples were collected through an in-dwelling cannula, and to avoid occlusion, heparinized saline was used for line flushing.

Image Acquisition and In Vivo Activity Measurement

Images were acquired on a Siemens Biograph 6 TruePoint PET/CT scanner (with TrueV; extended field of view) with 21.6-cm axial and 60.5-cm transaxial fields of view. Before administration of ^{18}F-ICMT-11, an attenuation CT scan of each subject was obtained from the vertex to mid thigh (CT settings: 130 kV; 15 effective mAs; pitch, 1.5; slice thickness, 5 mm; rotation time, 0.6 s; and effective dose [ED], 2.5 mSv). The CT scan was followed by 4 emission scans consisting of contiguous static images acquired at 6–7 bed positions, with the inferior border set to mid thigh and the superior border set at the vertex. The subjects were permitted to rise and move after this and were encouraged to void to enhance tracer clearance. After this break, a second attenuation CT scan and 2 further emission scans were obtained. In total, 6 emission scans were taken at time points up to 4 h after injection, with nominal start times of 0, 8, 22, 56, 121, and 170 min after injection. To compensate for physical decay of ^{18}F, the acquisition for each bed position was 1, 2, 5, 5, 7, and 7 min per individual bed position for these 6 time points after injection. The mean injected ^{18}F-ICMT-11 activity and ICMT-11 cold dose in the subjects were 159 ± 3 MBq (range, 154–161 MBq) and 2.18 ± 1.39 μg (range, 0.1–4.44 μg), respectively.

Emission data were reconstructed using the ordered-subsets expectation maximization algorithm (3 iterations and 21 subsets). Volumes of interest (VOIs) were delineated manually on the attenuation CT scan, using a circle of a fixed diameter, depending on the size of the organ. To avoid tissue inhomogeneity, particularly near organ boundaries, the VOIs were defined within the boundaries of the normal-tissue organs, as visualized on the CT images and mapped to the corresponding emission scans using shape-based interpolation to extract the ^{18}F activities with the ANALYZE analysis software (version 11; Biomedical Imaging Resource, Mayo Clinic). For the urinary bladder where the volume changes over time, the organ was outlined manually on the emission scans. All the volumes were outlined by a single investigator to avoid any interobserver variation. ^{18}F activity concentrations in the images were decay-corrected to the time of injection. VOIs included brain, thyroid, thymus, breast, lungs, heart wall, aortic lumen, liver, gallbladder, spleen, stomach wall, pancreas, adrenals, kidneys, small intestine wall and contents, large intestine wall and contents, urinary bladder contents, uterus, testes/ovaries, gluteus maximus muscle, and red marrow (iliac crest).

Measurement of Blood Activity

Venous blood samples were taken at nominal times of 5, 10, 15, 30, 60, 90, 150, and 240 min after injection. Single aliquots, each of whole blood and plasma, were obtained from each sample, and ^{18}F activity concentration was measured in a well counter previously cross-calibrated to the PET scanner. Urine was collected as voided up to 240 min after injection, and the volume and time of each micturition were recorded. Dual aliquots of urine were sampled from each void, and the mean ^{18}F activity was measured; the resulting ^{18}F activity concentration was multiplied by the volume of voided urine to provide the ^{18}F activity excreted.

Biodistribution and Dosimetry

For each subject and for each source region, the non–decay-corrected ^{18}F activity concentration over the 6 time points was generated. The integrated activity concentrations (area under the curve [AUC]) were calculated for all organ VOIs by applying a trapezoidal integration to the non–decay-corrected time–activity curves over the duration of the scan and the projection of decay in activity that was extrapolated beyond the last time point for imaging. The total number of disintegrations in each organ normalized to injected activity (subsequently referred to as the residence time [RT]: kBq·h·kBq^{-1}) was calculated as follows (Eq. 1):

$$\tau = \left(\mathrm{AUC} \times \mathrm{V}_{\mathrm{organ}}\right)/\text{injected activity}, \qquad \text{Eq. 1}$$

where τ is the RT, AUC is the area under the curve of the non–decay-corrected time–activity curve, and $\mathrm{V}_{\mathrm{organ}}$ is the tabulated organ volume as used in the OLINDA/EXM version 1.1 (*16*). As the volume of the urinary bladder and the gallbladder changed over time, the image-derived organ volume at each scan time point was used to estimate the RT, rather than the tabulated organ volume. Lung activity was corrected for tissue density using a density value of 0.33 g/mL (*17*). The tissue density in the other organs was assumed to be 1.0 g/mL. With the exception of the urinary bladder, extrapolation of the integration past the last image data point (4 h) assumed only physical decay of the ^{18}F label without biologic clearance—that is, an additional contribution to the AUC of time–activity curve_l/λ where time–activity curve_l is the last time–activity curve value measured and λ the decay constant for ^{18}F. For the bladder, the measured voided activities were also included to form an extended 8-time-point time–activity curve

(Supplemental Fig. 1; supplemental materials are available at http://jnm.snmjournals.org). The function:

$$A\left(1 - e^{-Bt}\right)e^{-Ct} - \sum_i A_i e^{-\lambda(t-t_i)} \qquad \text{Eq. 2}$$

was used to model the bladder time–activity curve where *A, B, C* are the estimated parameters, *t* the time since administration of the tracer, and A_i the urine radioactivity voided at time t_i (*18,19*). Residual bladder activity was not included in the model because it was not known if complete voiding had occurred for these subjects, although any residual activities must have been small, compared with the voided activities. The sum of the squared differences between the function and the extended time–activity curve was minimized for each subject using the solver function in Excel 2010 (Microsoft, Inc.). Across all 8 subjects, the AUCs derived from the fitted function matched the measured AUCs calculated above with a fractional mean difference of −3% and SD of 6%. The decay constant *C* is usually assumed to be the same as λ on physical grounds, but in this case a larger value was observed. This larger value may be attributed to activity becoming trapped in other tissues of the body, most notably the gallbladder. As a result, for *t* greater than 5 h, Equation 2 predicts a faster decline in bladder activity than is physically possible. This is, however, beyond the observation time in the present study for which the bladder activity accumulation rate was always positive and was predicted to be very small after 4 h. The fitted functions were extrapolated to estimate the bladder RT for each subject for the following voiding scenarios: complete bladder voids every hour, every 2 h, and every 4 h after tracer administration. Finally, the RT of the remainder term (assumed to be homogeneously distributed in the body) was obtained by subtracting the sum of all defined organ RTs from the inverse of the decay constant for ^{18}F.

The internal radiation dosimetry was evaluated through the RTs for the organs in each subject, provided as input to the OLINDA/EXM version 1.1 (*16*). The organ absorbed doses and ED for each individual subject were subsequently averaged. Because ICRP 103 (*20*) tissue-weighting factors (W_T) are not implemented in OLINDA/EXM 1.1, the male and female EDs are based on W_T from ICRP 60 (*21*).

An additional correction to the dose estimates arises because OLINDA/EXM 1.1 assumes that the stomach activity is all in the contents rather than the organ wall. The former was considered unlikely in this case. This only affects the β- (positron) contribution to the dose and is corrected by noting that the energy deposited in the wall from the contents is assumed within OLINDA/EXM to be half that calculated for the contents.

RESULTS

Safety

^{18}F-ICMT-11 was found to be safe and well tolerated in all subjects. No tracer-related serious AEs or AEs were observed in

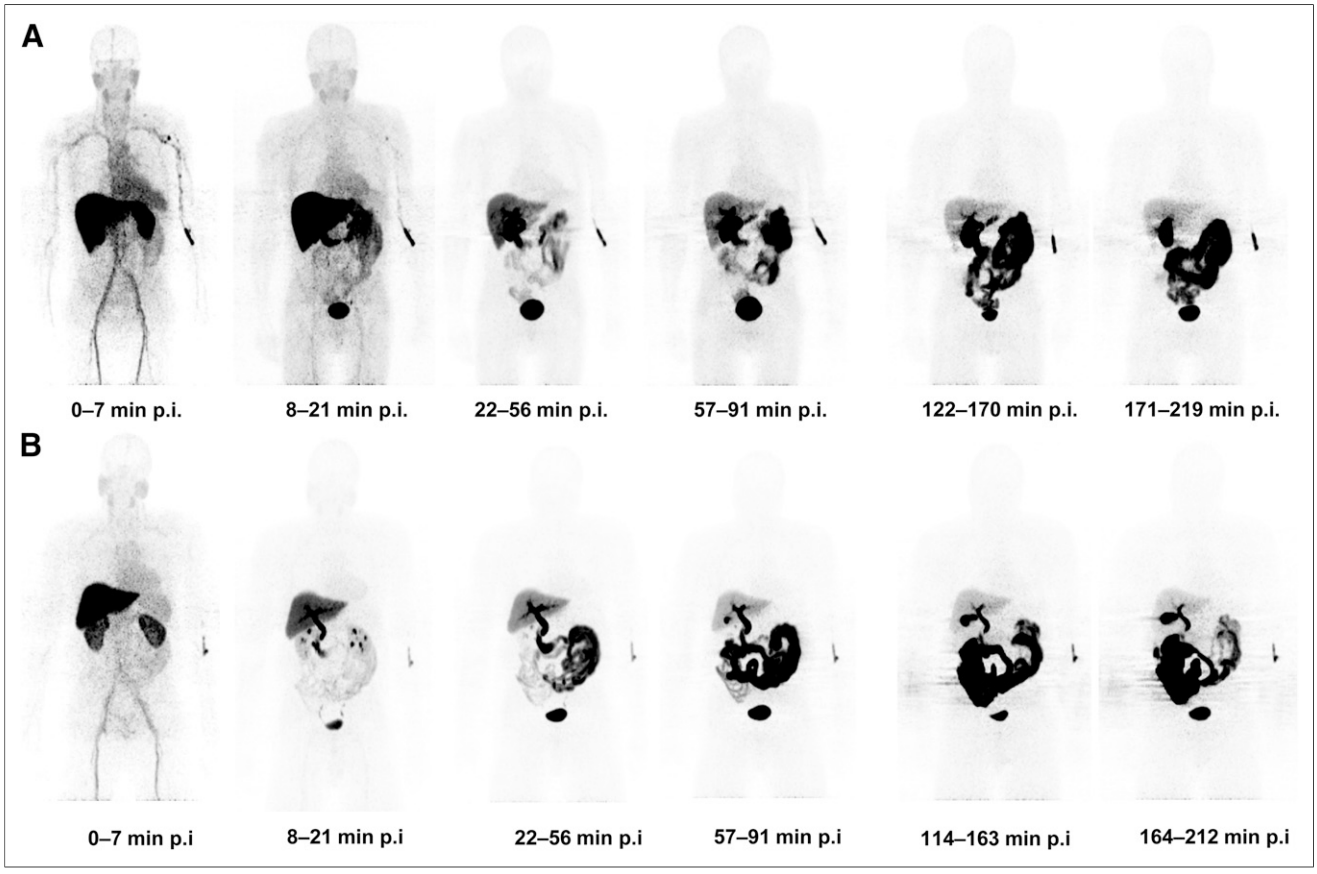

FIGURE 1. Series of whole-body maximum-intensity-projection images of representative subjects showing biodistribution of ^{18}F activity after tracer injection up to 219 min after injection of ^{18}F-ICMT-11. (A) Biodistribution of ^{18}F activity in subject who had meal 2–3 h before tracer injection. There is rapid clearance of radioactivity in cranium and thorax approximately 20 min after tracer injection and accumulation of radioactivity in gallbladder bowel from about 30 min after tracer injection. (B) Biodistribution of ^{18}F activity in subject who had meal just before tracer injection (due to delays in tracer production). Notable difference, compared with A, is reduced physiologic activity in liver at earlier time points and increased activity in bowel at later time points. p.i. = after injection.

relation to ^{18}F-ICMT-11 injection. Three of the 8 subjects had 4 non–tracer-related AEs (grade 1), including headache, transient blurring of vision, transient fluctuations in blood pressure, and neutropenia (associated with a concurrent eye infection), which resolved spontaneously within 24–48 h. No significant changes in vital signs, clinical laboratory blood tests, or electrocardiograms were observed. The safety results were reviewed by an independent data monitoring committee.

Biodistribution

After the administration of ^{18}F-ICMT-11, radioactivity was initially detected in the vascular compartment and then rapidly distributed to the liver and kidneys, followed by rapid elimination through the kidneys and the hepatobiliary system. About 18% of the injected activity (decay-corrected back to injection time) was eliminated within the first 4 h through the kidneys (9% in the first hour, 14% after 2 h). Radioactivity was already detectable in the urinary bladder at 8 min after tracer administration. The initial radioactivity uptake in the liver was gradually cleared approximately 3 h after injection. At about 30 min after the ^{18}F-ICMT-11 injection, there was a gradual increase in accumulation of radioactivity in the gallbladder and bowel. Typical images illustrating tracer uptake at various time points from 2 representative subjects are shown in Figure 1. Time–activity curves were generated for various organs (Fig. 2). There were no differences in the biodistribution profiles between men and women. The mean RTs for male and female subjects are summarized in Table 1. The RT contribution from the extrapolated part of the AUC beyond the last time point for imaging accounted for 40% of the total RT, contributing to 65% of the total ED and 57% of total EDE.

Dosimetry

Table 2 summarizes the mean organ absorbed dose estimates for ^{18}F-ICMT-11 injection. The mean ED averaged over both men and women was estimated to be 0.025 ± 0.004 mSv/MBq (men, 0.022 ± 0.004; women, 0.027 ± 0.004). The 5 organs receiving the highest absorbed dose (mGy/MBq), averaged over both men and women, were the gallbladder wall (0.59 ± 0.44), small intestine (0.12 ± 0.05), upper large intestinal wall (0.08 ± 0.07), urinary bladder wall (0.08 ± 0.02), and liver (0.07 ± 0.01). The values quoted are based on the 2-h bladder-voiding scenario, which is likely to be conservative in routine imaging scenarios where subjects would be encouraged to consume moderate quantities of fluids and empty their bladders regularly as done for ^{18}F-FDG studies. If the 4-h voiding scenario were used, this would increase the bladder wall absorbed dose by 64% (increase of 0.05 mGy/MBq: averaged for male and female subjects).

Effect of Food

Due to delays in tracer production and scan scheduling on the day of the scan, 3 of the 8 subjects had a meal just before tracer injection. Interestingly, in those 3 subjects, the distribution of radioactivity in the abdomen was notably different when compared with the other subjects (Fig. 1B). The intake of food has reduced physiologic activity in the liver at earlier time points and increased activity in the bowel (changed the absorbed dose as follows: stomach [5% decrease], small intestine [79% increase], upper large intestine [197% increase], and lower large intestine [25% increase]) at later time points. This is consistent with normal postprandial physiology, with emptying of gallbladder content (bile juice) to aid digestion. This increased bowel activity is also demonstrated in the time–activity curve profiles of the elimination organs (Supplemental Fig. 2). However, there was no difference in the other organs and in the plasma ^{18}F activity concentrations.

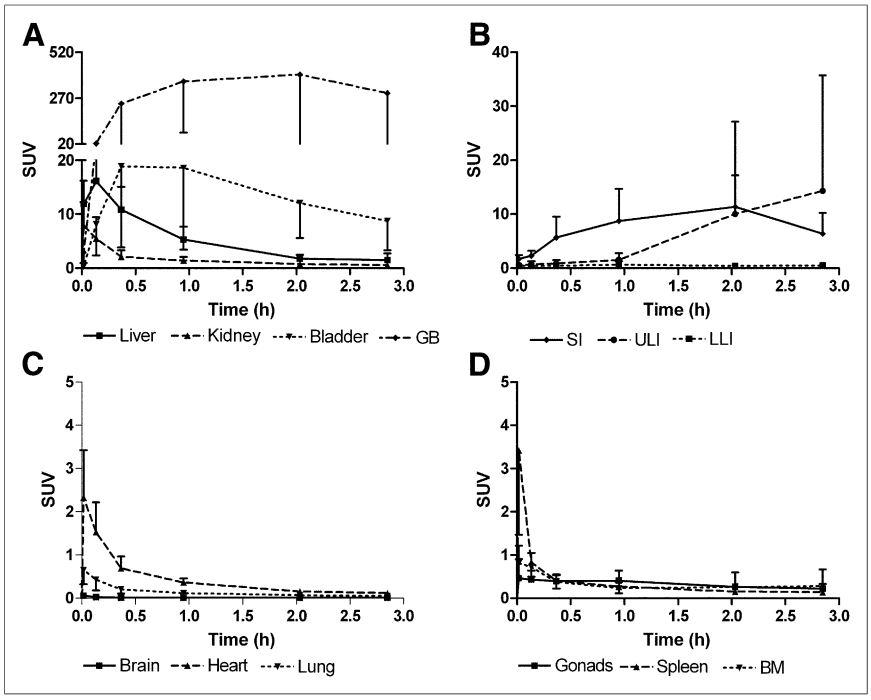

FIGURE 2. Mean non–decay-corrected time–activity curves normalized to injected activity (kBq) and body weight (g) for ^{18}F-ICMT-11. Time–activity curves were generated for several organs at various time points up to 4 h after tracer administration in elimination organs (renal and hepatobiliary system) (A), bowel (small intestine and upper and lower large intestine) (B), cranium and thorax (C), and organs with potential physiologic apoptosis (gonads, spleen, and bone marrow) (D). Error bars represent 1 SD from mean and are shown 1-sided for clarity. BM = bone marrow; GB = gallbladder; SI = small intestine; LLI = lower large intestine; ULI = upper large intestine.

DISCUSSION

We have shown in this first-in-human study that the caspase-3–specific apoptosis imaging agent ^{18}F-ICMT-11 is safe and well tolerated. Injection of ^{18}F-ICMT-11 led to rapid washout of the ^{18}F activity from the vascular compartment and elimination primarily via the renal and hepatobiliary routes. Renal excretion (18% in 4 h) was comparably lower than for routinely used radiotracers such as ^{18}F-FDG (30%) (*22,23*) and ^{18}F-fluorodihydroxyphenylalanine (31%) (*24*). In contrast, tracer localization within the gallbladder was relatively high, with slow washout into the gastrointestinal tract.

We determined the mean ED of ^{18}F-ICMT-11 as 0.025 mSv/MBq, which is comparable with the ED of ^{18}F-FDG

TABLE 1
Mean RTs (τ) of ^{18}F-ICMT-11 for Different Organs in Male (n = 4) and Female (n = 4) Volunteers

	RT (τ) (kBq·h·kBq^{-1})			
	Men		Women	
Organ	Mean	SD	Mean	SD
Adrenal	0.001	0.0001	0.001	0.001
Bladder*	0.127	0.020	0.120	0.033
Brain	0.001	0.0004	0.001	0.0003
Breast			0.004	0.002
Gallbladder	0.369	0.407	0.321	0.143
Heart contents	0.006	0.001	0.005	0.0004
Heart wall	0.006	0.002	0.004	0.001
Kidney	0.021	0.004	0.019	0.011
Liver	0.381	0.062	0.351	0.130
Lower large intestine	0.004	0.001	0.005	0.004
Lung†	0.018	0.007	0.012	0.007
Muscle	0.255	0.025	0.170	0.043
Ovaries‡			0.0003	0.00002
Pancreas	0.007	0.006	0.005	0.005
Red marrow	0.026	0.022	0.013	0.003
Small intestine	0.449	0.202	0.514	0.306
Spleen	0.003	0.0004	0.002	0.001
Stomach	0.005	0.002	0.003	0.001
Testis	0.001	0.0001		
Thyroid	0.000	0.00004	0.0001	0.00003
Upper large intestine	0.214	0.242	0.039	0.064
Uterus			0.005	0.001
Thymus	0.0001	0.00003	0.0003	0.0001
Remainder	0.745	0.321	1.059	0.200

*Bladder RT is for 2-h voiding scenario.
†Lung activity was corrected for tissue density value of 0.33 g/mL and other organs with density value of 1 g/mL.
‡In 2 subjects, ovaries were not visible due to postmenopausal atrophy.

(0.019 mSv/MBq) (*22*). The dose limits specified in the Code of Federal Regulations (*25*) per single administration of a radioactive drug for research purposes are 30 mSv to the whole body, blood-forming organs, lens of the eye, and gonads, with a maximum annual dose of 50 mSv. The maximum allowable single and annual doses to all other organs are 50 and 150 mSv, respectively (*25*). If we assume a 370-MBq administered radioactivity for ^{18}F-ICMT-11 (typical of many PET tracers), the ED would be 9.3 mSv. For this administered radioactivity level, the equivalent dose received by the gonads would be estimated as 1.9 mSv. These are well within the dose limits specified.

Regarding radiotracer uptake in normal adult tissues with potentially high intrinsic apoptosis, we did not see high ^{18}F-ICMT-11 uptake in the testes. Apoptosis plays a significant role in normal testicular physiology and up to 75% of the spermatogonia die by apoptosis before reaching maturity, thus regulating sperm production, a phenomenon that is accentuated in patients with infertility (*26*). The biodistribution study of ^{18}F-ML-10, a small-molecule apoptotic tracer, demonstrated a distinct pattern of uptake in the testes (*27*). However, the biodistribution studies of annexin-V–based radiotracers (^{99m}Tc-annexin-V, ^{99m}Tc-hydrazino nicotinate [HYNIC]-annexin-V, and ^{99m}Tc-4, 5-bis [thioacetoamide] pentanoyl [BTAP]-annexin-V) did not show increased uptake in the testes, with the absorbed dose in the testes ranging from 0.005 to 0.015 mGy/MBq (*28–30*). This dose is comparable to the absorbed testes dose observed with ^{18}F-ICMT-11 (0.007 mGy/MBq). The significantly increased uptake of ^{18}F-ML-10 in the testes could be attributed to the young age of the male volunteers enrolled in the study (mean age, 23 y; range, 21–44 y). The average age of the male volunteers in the ^{99m}Tc-annexin-V and ^{99m}Tc-BTAP-annexin-V biodistribution studies was 53 y, which is comparable to the age range in our study (63.1 ± 2.58 y; range, 59–68 y). There is a strong relationship between testicular apoptotic index and age (*31,32*), with a reduction in semen volume by nearly 50% and reduced sperm production (*33*) with increasing age. This relationship suggests a decrease in the physiologic apoptosis with increasing age, which could explain the lack of significant uptake seen in the testes with ^{18}F-ICMT-11.

There was uptake of ^{18}F-ICMT-11 in the bone marrow, with a mean absorbed dose of 0.012 mGy/MBq. This dose is comparable to that of ^{99m}Tc-HYNIC-annexin-V (0.004–0.008 mGy/MBq) (*30,34*), suggesting that the marrow uptake was physiologic, because apoptotic cell death is a physiologic component of normal hematopoiesis (*35*).

Although no specific instructions were given to the subjects to fast before the scan, in 3 of the subjects who had a meal before the scan, there was notably reduced physiologic activity in the liver at earlier time points and increased activity in the bowel at later

TABLE 2
Mean Organ Absorbed Dose Estimates Expressed in mGy/MBq for ^{18}F-ICMT-11 (n = 8) with Bladder-Voiding Scenarios

	Mean absorbed dose estimates (mGy/MBq)			
	2-h voiding scenario		4-h voiding scenario	
Organ	Mean	SD	Mean	SD
Adrenals	0.022	0.005	0.022	0.005
Brain	0.003	0.001	0.002	0.001
Breasts	0.006	0.001	0.006	0.001
Gallbladder wall	0.594	0.446	0.593	0.446
Lower large intestine wall	0.021	0.006	0.022	0.006
Small intestine	0.122	0.056	0.122	0.056
Stomach wall	0.023	0.003	0.022	0.003
Upper large intestine wall	0.084	0.071	0.084	0.071
Heart wall	0.012	0.001	0.012	0.001
Kidneys	0.027	0.005	0.027	0.005
Liver	0.065	0.016	0.065	0.016
Lungs	0.010	0.002	0.010	0.002
Muscle	0.010	0.001	0.010	0.001
Ovaries	0.025	0.007	0.026	0.007
Pancreas	0.029	0.008	0.029	0.008
Red marrow	0.012	0.001	0.012	0.001
Osteogenic cells	0.012	0.003	0.012	0.003
Skin	0.006	0.001	0.006	0.001
Spleen	0.011	0.001	0.011	0.001
Testes	0.007	0.000	0.008	0.000
Thymus	0.007	0.001	0.007	0.001
Thyroid	0.005	0.001	0.005	0.001
Urinary bladder wall	0.080	0.019	0.131	0.031
Uterus	0.028	0.009	0.030	0.009
Total body	0.013	0.002	0.013	0.002
Mean ED (mSv/MBq)	0.025	0.004	0.026	0.004

time points. The impact of food appeared to be restricted to the hepatobiliary and intestinal elimination organs because no differences in the time–activity curves from other organs or the plasma ^{18}F radioactivity were observed. This interesting observation suggests that abdominal imaging could be facilitated by incorporating a standard prescan meal or a promotility agent to help clear out the bowel activity and improve the signal-to-background ratio.

In summary, ^{18}F-ICMT-11 injection is safe and well tolerated, with a favorable dosimetry profile in healthy volunteers. Organ dose estimates are similar to those seen with other routine ^{18}F-labeled tracers. The potential risks due to radiation are within accepted limits. Further clinical studies are now warranted to evaluate the utility of ^{18}F-ICMT-11 in measuring the effects of treatment on tumor apoptosis.

CONCLUSION

^{18}F-ICMT-11 is a safe PET tracer, with a favorable radiation dosimetry profile for clinical imaging. The ED is 0.025 ± 0.004 mSv/MBq, which is within the range of other common ^{18}F PET tracers.

DISCLOSURE

The costs of publication of this article were defrayed in part by the payment of page charges. Therefore, and solely to indicate this fact, this article is hereby marked "advertisement" in accordance with 18 USC section 1734. This work was supported by the U.K. Medical Research Council (MRC) grant MC-A652-5PY80, the Joint Cancer Research U.K., and the Engineering and Physical Sciences Research Council Cancer Imaging Centre at Imperial College London, in association with the MRC and Department of Health (England) grant C2536/A10337, Experimental Cancer Medicine Centers grant C37/A7283, and National Institute for Health Research (NIHR) Biomedical Research Centre award to Imperial College Healthcare NHS Trust and Imperial College London. This work was also supported by an NIHR Clinician Scientist Award (LMK;012/009). EOA's laboratory is member of the European Commission Innovative Medicines Initiative QuIC-ConCePT consortium. No other potential conflict of interest relevant to this article was reported.

ACKNOWLEDGMENTS

We thank the healthy volunteers, staff of Imanova Ltd., and staff of NIHR/Wellcome Trust Imperial Clinical Research Facility for their support of the trial.

REFERENCES

1. Degterev A, Boyce M, Yuan J. A decade of caspases. *Oncogene.* 2003;22:8543–8567.
2. Nicholson DW, Thornberry NA. Caspases: killer proteases. *Trends Biochem Sci.* 1997;22:299–306.
3. Okada H, Mak TW. Pathways of apoptotic and non-apoptotic death in tumour cells. *Nat Rev Cancer.* 2004;4:592–603.
4. Reed JC. Apoptosis-based therapies. *Nat Rev Drug Discov.* 2002;1:111–121.
5. Hanahan D, Weinberg RA. The hallmarks of cancer. *Cell.* 2000;100:57–70.
6. Taylor RC, Cullen SP, Martin SJ. Apoptosis: controlled demolition at the cellular level. *Nat Rev Mol Cell Biol.* 2008;9:231–241.
7. Porter AG, Janicke RU. Emerging roles of caspase-3 in apoptosis. *Cell Death Differ.* 1999;6:99–104.
8. Chang J, Ormerod M, Powles TJ, Allred DC, Ashley SE, Dowsett M. Apoptosis and proliferation as predictors of chemotherapy response in patients with breast carcinoma. *Cancer.* 2000;89:2145–2152.
9. Dubray B, Breton C, Delic J, et al. In vitro radiation-induced apoptosis and early response to low-dose radiotherapy in non-Hodgkin's lymphomas. *Radiother Oncol.* 1998;46:185–191.
10. Faried A, Sohda M, Nakajima M, Miyazaki T, Kato H, Kuwano H. Expression of heat-shock protein Hsp60 correlated with the apoptotic index and patient prognosis in human oesophageal squamous cell carcinoma. *Eur J Cancer.* 2004;40:2804–2811.
11. Jia Y, Dong B, Tang L, et al. Apoptosis index correlates with chemotherapy efficacy and predicts the survival of patients with gastric cancer. *Tumour Biol.* 2012;33:1151–1158.
12. Eisenhauer EA, Therasse P, Bogaerts J, et al. New response evaluation criteria in solid tumours: revised RECIST guideline (version 1.1). *Eur J Cancer.* 2009;45:228–247.
13. Nguyen QD, Challapalli A, Smith G, Fortt R, Aboagye EO. Imaging apoptosis with positron emission tomography: 'bench to bedside' development of the caspase-3/7 specific radiotracer [^{18}F]ICMT-11. *Eur J Cancer.* 2012;48:432–440.
14. Nguyen QD, Smith G, Glaser M, Perumal M, Arstad E, Aboagye EO. Positron emission tomography imaging of drug-induced tumor apoptosis with a caspase-3/7 specific [^{18}F]-labeled isatin sulfonamide. *Proc Natl Acad Sci USA.* 2009;106:16375–16380.
15. Fortt R, Smith G, Awais RO, Luthra SK, Aboagye EO. Automated GMP synthesis of [^{18}F]ICMT-11 for in vivo imaging of caspase-3 activity. *Nucl Med Biol.* 2012;39:1000–1005.
16. Stabin MG, Sparks RB, Crowe E. OLINDA/EXM: the second-generation personal computer software for internal dose assessment in nuclear medicine. *J Nucl Med.* 2005;46:1023–1027.
17. Rhodes CG, Wollmer P, Fazio F, Jones T. Quantitative measurement of regional extravascular lung density using positron emission and transmission tomography. *J Comput Assist Tomogr.* 1981;5:783–791.
18. Graham MM, Peterson LM, Link JM, et al. Fluorine-18-fluoromisonidazole radiation dosimetry in imaging studies. *J Nucl Med.* 1997;38:1631–1636.
19. Thomas SR, Stabin MG, Chen CT, Samaratunga RC. MIRD pamphlet no. 14 revised: a dynamic urinary bladder model for radiation dose calculations. Task Group of the MIRD Committee, Society of Nuclear Medicine. *J Nucl Med.* 1999;40:102S–123S.
20. The 2007 recommendations of the International Commission on Radiological Protection. ICRP publication 103. *Ann ICRP.* 2007;37:1–332.
21. 1990 recommendations of the International Commission on Radiological Protection. ICRP publication 60. *Ann ICRP.* 1991;21:1–201.
22. Radiation dose to patients from radiopharmaceuticals (addendum 2 to ICRP publication 53). ICRP publication 80. *Ann ICRP.* 1998;28:1–126.
23. Jones SC, Alavi A, Christman D, Montanez I, Wolf AP, Reivich M. The radiation dosimetry of 2 [F-18]fluoro-2-deoxy-D-glucose in man. *J Nucl Med.* 1982;23:613–617.
24. Brown WD, Oakes TR, DeJesus OT, et al. Fluorine-18-fluoro-L-DOPA dosimetry with carbidopa pretreatment. *J Nucl Med.* 1998;39:1884–1891.
25. Radioactive drugs for certain research uses. Code of Federal Regulations Title 21, Part 361.1. http://www.accessdata.fda.gov/scripts/cdrh/cfdocs/cfcfr/CFRSearch.cfm?fr=361. Accessed July 16, 2013.
26. Martincic DS, Virant Klun I, Zorn B, Vrtovec HM. Germ cell apoptosis in the human testis. *Pflugers Arch.* 2001;442:R159–R160.
27. Höglund J, Shirvan A, Antoni G, et al. ^{18}F-ML-10, a PET tracer for apoptosis: first human study. *J Nucl Med.* 2011;52:720–725.
28. Kemerink GJ, Boersma HH, Thimister PW, et al. Biodistribution and dosimetry of ^{99m}Tc-BTAP-annexin-V in humans. *Eur J Nucl Med.* 2001;28:1373–1378.
29. Kemerink GJ, Liem IH, Hofstra L, et al. Patient dosimetry of intravenously administered ^{99m}Tc-annexin V. *J Nucl Med.* 2001;42:382–387.
30. Kemerink GJ, Liu X, Kieffer D, et al. Safety, biodistribution, and dosimetry of ^{99m}Tc-HYNIC-annexin V, a novel human recombinant annexin V for human application. *J Nucl Med.* 2003;44:947–952.
31. Ng KK, Donat R, Chan L, Lalak A, Di Pierro I, Handelsman DJ. Sperm output of older men. *Hum Reprod.* 2004;19:1811–1815.
32. Schmelz HU, Meiswinkel J, Port M, et al. Apoptosis in non-tumorous adult human testis tissue: comparison of so-called 'normal' testis tissues. *Urol Int.* 2005;74:349–354.
33. Johnson L. Spermatogenesis and aging in the human. *J Androl.* 1986;7:331–354.
34. Ohtsuki K, Akashi K, Aoka Y, et al. Technetium-99m HYNIC-annexin V: a potential radiopharmaceutical for the in-vivo detection of apoptosis. *Eur J Nucl Med.* 1999;26:1251–1258.
35. Domen J. The role of apoptosis in regulating hematopoiesis and hematopoietic stem cells. *Immunol Res.* 2000;22:83–94.